https://doi.org/10.15360/1813-9779-2026-2-2644

The Beneficial Effects of Krypton Inhalation Following Traumatic Brain Injury in Rats

Viktoriya V. Antonova*, Dmitry V. Kuidin, Ekaterina A. Boeva, Rostislav A. Cherpakov, Maxim A. Lyubomudrov, Zoya I. Tsokolaeva, Sergey N. Kalabushev

Federal Research and Clinical Center of Intensive Care Medicine and Rehabilitology, Ministry of Education and Science of Russia, 25 Petrovka Str., Bldg. 2, 107031 Moscow, Russia

For citation: *Viktoriya V. Antonova, Dmitry V. Kuidin, Ekaterina A. Boeva, Rostislav A. Cherpakov, Maxim A. Lyubomudrov, Zoya I. Tsokolaeva, Sergey N. Kalabushev.* The Beneficial Effects of Krypton Inhalation Following Traumatic Brain Injury in Rats. *Obshchaya Reanimatologiya = General Reanimatology.* 2026; 22 (2): 38–49. https://doi.org/10.15360/1813-9779-2026-2-2644 [In Russ. and Engl.]

***Correspondence to:** Viktoriya V. Antonova, victoryant.sci@gmail.com

Summary

Traumatic brain injury (TBI) remains one of the leading causes of disability, and current approaches to neuroprotection have limited efficacy. The inert gas krypton is considered a promising neuroprotective agent; however, data on its effects in TBI and on components of the neurovascular unit (NVU) are limited.

Objective. To evaluate the neuroprotective potential of krypton in rats with traumatic brain injury (TBI) *in vivo* and in NVU cell cultures subjected to oxygen-glucose deprivation (OGD) *in vitro*.

Materials and Methods. The study included 48 Wistar rats divided into 3 groups: SO (sham operated), TBI (N_2/O_2 70/30 %), and TBI + iKr (Kr/O_2 70/30 %). A model of controlled open brain contusion injury was used. On day 14, we assessed neurological deficits (limb placing test, LPT), the extent of brain injury (T2-weighted MRI slices), morphological changes (hematoxylin-eosin staining), and the expression of GFAP and Caspase-3 (fluorescent immunohistochemistry, IHC). IL-1β, IL-6, and TNF-α mRNA levels in the injury zone were determined by PCR. *In vitro* studies investigated the effect of krypton preconditioning (Kr/O_2 79/21 %, 24 h) on the survival of neuronal (SH-SY5Y), glial (C6), and vascular endothelial (Ea.Hy926) cells during OGD (4–6 h).

Results. A significant neurological deficit of 2.5 (2; 5.25) scores was determined by the TBI modeling accompanied by a large volume of brain damage of 33 (28; 39) mm³. Krypton inhalation led to a reduction in the lesion volume to 18 (15; 26) mm³ and accelerated the recovery of sensorimotor functions: starting on day 7, the indicators in the TBI + iKr group were statistically significantly better than in the TBI group, and by day 14, they approached the values of the SO (control) group. In the TBI + iKr group, IL-1β and TNF-α levels in the affected hemisphere were nearly 50% lower than in the TBI group, while remaining higher than in the SO group; changes in IL-6 levels were insignificant. Histologically, less significant cerebral edema, spongiosis, and neuronal degeneration were observed in the TBI + iKr group. Immunohistochemical analysis revealed a trend toward more pronounced reactive gliosis (GFAP) with no differences in Caspase-3. *In vitro*, krypton preconditioning under OGD conditions did not improve the survival of neuronal, glial, and endothelial cells.

Conclusion. Krypton exerted significant neuroprotective effect in experimental TBI in rats, reducing neurological deficits, the extent of structural damage, and the severity of the inflammatory response. The absence of a protective effect in NVU cellular models underscores the essential role of systemic and intercellular interactions in the neuroprotective action of krypton and warrants further research into its mechanisms of action and dosing optimization.

Keywords: krypton; traumatic brain injury; in vitro neuroprotection; oxygen-glucose deprivation

Conflict of interest. The authors declare no conflict of interest.

Information about the authors:
Viktoriya V. Antonova: https://orcid.org/0000-0002-0819-7886
Dmitry V. Kuidin: https://orcid.org/0009-0008-2902-9962
Ekaterina A. Boeva: https://orcid.org/0000-0002-0422-5018
Rostislav A. Cherpakov: https://orcid.org/0000-0002-0514-2177
Maxim A. Lyubomudrov: https://orcid.org/0000-0002-1735-592X
Zoya I. Tsokolaeva: https://orcid.org/0000-0003-2441-6062
Sergey N. Kalabushev: https://orcid.org/0000-0001-7017-7897

Introduction

The brain is one of the most protected yet most vulnerable organs. Brain injury may commonly result in catastrophic consequences, both for the individual and a whole society, placing a significant burden on the healthcare system, the social sector, and the economy [1]. In this regard, developing strategies aimed at preserving brain structure and functions is one of the priorities of current critical care practice [2]. In this context, numerous strategies have been developed to minimize the consequences of brain injury, including the prevention and treatment of intracranial hypertension, ensuring adequate oxygen and nutrient delivery, and reducing energy deficit [3–7]. However, given current data on the pathogenesis of brain injuries associated with trau-

matic brain injury (TBI) and their contribution to the development of delayed neurocognitive disorders even with a favorable treatment outcome, the measures currently in use are insufficient [8].

In this regard, it seems timely to seek new strategies for preventing and mitigating the consequences of TBI that will complement existing approaches. One such strategy could be the use of so-called «neuroprotectants». This term currently refers to a group of substances capable of influencing key molecular mechanisms in the pathogenesis of neurotrauma and reducing the extent of damage to the neurovascular unit (NVU) [9].

Numerous neuroprotective agents have been synthesized and tested in the past, but none of them are sufficiently effective, and some turned to be even harmful during the acute phase of neurotrauma [10–12]. Unlike pharmacological agents, which generally have limited bioavailability and low ability to cross the blood-brain barrier, inert gases possess a number of properties that are attractive for neuroprotection [13–19].They have extremely low chemical reactivity, enter and leave the body unchanged without forming metabolites, yet they possess relatively high biological activity.

For example, the inert gas xenon possesses anesthetic and analgesic properties and is used in anesthesiology and for the relief of pain [20-22]. Helium has long been used in the treatment of conditions associated with bronchial obstructive syndrome [23, 24], while argon has shown promise in preclinical studies as an organ protector in conditions associated with ischemia-hypoxia and «no-reflow» syndromes (i.e., failed or insufficient microcirculation recovery in tissues after removal of main blood stream occlusion). The primary focus of research in this area is neuroprotection [25, 26]. As a neuroprotective agent, argon offers a number of advantages: it targets key mechanisms in brain injury pathogenesis, does not produce sedative effect under normobaric conditions, and does not require specialized inhalation equipment in experimental setting [27, 28].

In reference to TBI, the evidence regarding argon's neuroprotective properties remains inconclusive. Depending on the injury model, the severity of the trauma, and the therapeutic window, the effect of argon ranges from moderate to completely absent [29, 30]. Krypton, on the other hand, remains the least studied substance («dark horse») in the context of organ protection.

In early *in vitro* studies, krypton did not demonstrate any cytoprotective effects. However, a distinct neuroprotective effect was observed in our recent study using a model of photochemically induced stroke. The effect of krypton on the activation of Nrf2 and Akt, the inactivation of GSK-3β, and the suppression of NF-κB expression has been demonstrated [31, 32]. These proteins are involved in signaling pathways responsible for universal neuroprotective mechanisms, which may be sufficient to prevent secondary damage following TBI.

Objective: To evaluate the neuroprotective potential of krypton in rats with traumatic brain injury (TBI) *in vivo* and in NVU cell cultures subjected to OGD subjected to oxygen-glucose deprivation (OGD) *in vitro*.

Materials and Methods

The study was conducted in accordance with established national and international bioethical standards (Directive 2010/63/EU). The study protocol was approved by the Local Ethics Committee of the Federal Research and Clinical Center of Intensive Care Medicine and Rehabilitology No. 3/22/6 on December 14, 2022.

Study design: a prospective, randomized, controlled, experimental *in vivo* study with concurrent *in vitro* component.

Experimental animals. The study used 48 sexually mature male Wistar rats weighing 250–350 g. A total of 33 animals were included in the main protocol for simulating TBI. The animals were randomized into 3 groups: sham-operated (SO, $n=6$), TBI group ($n=11$), and TBI with krypton inhalation (TBI+iKr, $n=16$). Analysis of long-term neurological and morphological outcomes was performed on a per-protocol basis. It included only animals that completed the 14-day observation period without complications: SO group — $n=6$, TBI group — $n=8$, TBI+iKr group — $n=10$.

In addition, an independent subgroup ($n=15$) was formed and used exclusively for Western blotting without analysis of long-term outcomes. This subgroup included intact animals ($n=5$), animals from the TBI group ($n=5$), and animals from the TBI+iKr group ($n=5$).

Animals were assigned to groups using a random number generator (simple randomization). Sample size was calculated for the primary endpoint. The uneven distribution of animals among groups was stipulated by the study protocol. The larger size of the TBI+iKr group was due to the expected greater variability of the parameters and the need to ensure sufficient statistical power (80% at $\alpha=0.05$) to detect a potential neuroprotective effect. The number of animals in the SO group was minimized in accordance with the 3R principles (Reduction), since no significant variability in the studied parameters was expected in this group.

The researchers who conducted the neurological testing, MRI morphometry, and IHC analysis were blinded to the animals' group assignments.

The primary endpoint was the volume of brain damage as determined by MRI on day 14.

The secondary endpoints were: neurological deficits, levels of pro-inflammatory cytokines, the extent of GFAP and caspase-3 expression, and survival rates.

Traumatic brain injury modeling. Traumatic brain injury modeling was performed according to the method of controlled contusion injury to the exposed brain [33], which had previously been used in similar experiments. Main steps: after induction of anesthesia and shaving of the surgical field, a midline skin incision was made, and a trepanation hole (5 mm in diameter) was drilled above the sensorimotor cortex of the left hemisphere (2.5 mm lateral to the sagittal suture, 1.5 mm caudal to the bregma), and the injury was inflicted by an impact tip/striker placed over the dura mater. The wound was sutured, and the animal was placed under an infrared lamp with a thermoregulatory system to maintain a body temperature of 37 ± 0.5°C. In the SO group, a similar trepanation was performed without applying a blow [33].

Krypton treatment. Inhalations were performed after the animals awoke from anesthesia (90 minutes after TBI induction), 24 hours after TBI, and 48 hours after TBI (time points D0, D1, and D2, respectively); each inhalation session lasted 120 minutes. A semi-closed exposure system was used to administer the krypton-oxygen gas mixture, consisting of a transparent sealed chamber (35 L) with inlet and outlet ports for gas delivery and removal, a recirculation loop with a cooler, a drying system (silica gel), and a CO_2 absorption system (sodium lime), as well as an exhalation valve and an APL valve for releasing excess pressure. Environmental parameters were monitored using temperature, humidity, and gas concentration (O_2, Kr) sensors installed in the circuit. The gas supply was provided by mixtures from cylinders containing Kr/O_2 (70/30%) («KrypOxA 70/30», Akela-N LLC, Moscow, Russia) and N_2/O_2 (70/30%) («Nitrogen-Oxygen 70/30», «Akela-N» LLC, Moscow, Russia) mixtures via regulators and flow switches. All components were connected using standard rubber tubing and plastic fittings.

Assessment of neurological status. Neurological testing was conducted in accordance with the previously described protocol developed by De Ryck et al. [34] and subsequently modified by J. Jolkkonen et al. [35], which has also been used in a number of previous studies [29, 31, 36].

Prior to testing, the animals were acclimated to handling daily for seven days to reduce their stress response to manipulation. The assessment consisted of a series of seven behavioral tasks designed to analyze the sensorimotor integration of the forelimbs and hindlimbs in response to visual, tactile, and proprioceptive stimuli [36].

MRI examination. On the 14th day following traumatic brain injury, the animals underwent magnetic resonance imaging. A high-field MRI scanner with a magnetic field strength of 7 T and a gradient system up to 105 mT/m (BioSpec 70/30 model, Bruker, Germany) was used. Anesthesia was administered via inhalation with isoflurane at a concentration of 1.5–2%. The animals were secured in a special apparatus that provided stereotactic positioning and body temperature control [37].

A standard protocol for imaging brain structures in rodents, based on the acquisition of T2-weighted images and described in a previous publication [36], was applied.

Cytokine mRNA quantification by real-time PCR. The day after the final inhalation, decapitation was performed under anesthesia with 6% chloral hydrate at a dose of 300 mg/kg, followed by craniotomy and removal of the cerebral hemispheres. Cytokine mRNA levels were assessed by quantifying mRNA in rat brain for the pro-inflammatory cytokine genes IL-1β, IL-6, and TNF-α using real-time PCR.

RNA was isolated using the RNeasy MiniKit (QIAGEN, USA) according to the manufacturer's protocol.

Primers for PCR were selected using the Beacon Designer software. The primer pairs used are shown in Table 1.

Real-time PCR was performed in a BioRad iCycler (USA) amplifier according to the protocol (Table 2) using a mixture with the following composition: Mixture B (intercalating dye Eva Green + recessive dye ROX + Taq Pol + 25 mM dNTP + buffer («Sintol»)) — 10 µL, primers (mixture of 10 µM forward and reverse primers — 0.5 µL, MQ — 9.5 µL, reverse transcription product — 5 µL).

Histological analysis. On the 14th day after TBI, the rats' brains were fixed in 10% formalin, embedded in paraffin, and sectioned into 4-µm-thick slices. The sections were deparaffinized in xylene and rehydrated in an ethanol gradient. Antigen retrieval was performed at high temperature in citrate buffer, pH 6.0 (Target Retrieval Solution, DAKO). The sections were cooled, washed three times in PBS (with buffer + Tween; Cell Marque) for 5 minutes each, and incubated in 3% H_2O_2 for 10 minutes to block endogenous peroxidase activity. To prevent nonspecific binding, Protein Block Serum-Free (Abcam) was used for 30 minutes. The sections were incubated at 37°C for 1 hour with primary antibodies against Caspase-3 (1 : 100; ab13847, Abcam) and GFAP (1:500; 556329, BD Pharmingen, San Jose, CA), diluted in Antibody Diluent (ab64211; Abcam). The sections were then washed twice in PBS, stained with hematoxylin, washed again, and mounted under a cover slip. Secondary antibodies from the Dako REAL EnVision Detection System (DAB) or the ImmPACT Vector Red Substrate Kit, Alkaline Phosphatase (AP) (SK-5105) were applied according to the instructions. The sections were dehydrated in 70%, 96%, and 100% ethanol and cleared twice in xylene. Images were acquired using a Nikon

Table 1. Sequences and key characteristics of the primers used for real-time PCR.

Gene	Animal	Primer sequences (forward and reverse), 5' – 3'	Annealing temperature, °C
18S rRNA	Rat	GACAGGATTGACAGATTGAT	56
		TTATCGGAATTAACCAGACAA	
TNF-α	Rat	TTATCTACTCCCAGGTTCT	56
		TGGTATGAAATGGCAAATC	
IL-1beta	Rat	AGAACATAAGCCAACAAGT	56
		ACACAGGACAGGTATAGAT	
IL-6	Rat	TGATTGTATGAACAGCGATGATG	56
		CCAGAAGACCAGAGCAGATT	
		TCACATCACAGTAGGAAGTT	

Note. Reverse transcription was performed using the SuperScript III kit provided by Thermo Scientific (USA).

Table 2: Real-time PCR protocol.

Period	Time	Temperature, °C	Number of cycles
Initiation	5 min	95	1
Denaturation	1 min	95	45
Annealing	20 s	56	
Elongation (stage 1)	20 s	72	
Elongation (stage 2)	1 min	72	1
Obtaining the melting curve	30 s	Every 30 seconds, the temperature rises by 0.5 °C	45

Note. For statistical analysis, the expression analysis results were normalized to 18S rRNA gene expression.

Eclipse Ni-e microscope and analyzed using NIS-Elements (Nikon) and ImageJ (NIH) software.

Modeling of the neurovascular unit. Intertwined cultures of glial cells (C6), neuronal cells (SH-SY5Y), and vascular endothelial cells (Ea.Hy926) were thawed from stock solutions in a water bath at 37°C, then resuspended in complete culture medium (CCM). For C6 cells, the medium consisted of DMEM containing 1 g/L glucose + F12 (1:1) with 5% fetal bovine serum (FBS), 1% L-glutamine, and 1% antibiotics (penicillin, streptomycin). For SH-SY5Y cells — DMEM containing 1 g/L glucose + F12 (1:1) with 20% fetal bovine serum (FBS), 1% L-glutamine, and 1% antibiotics (penicillin, streptomycin). For Ea.Hy926 cells — DMEM containing 1 g/L glucose + F12 (1:1) with 5% fetal bovine serum (FBS), 1% L-glutamine, 2% hypoxanthine and thymidine (HT). Culture conditions in a CO_2 incubator: 5% CO_2, 37°C. Once a monolayer was formed, the cells were passaged using a 0.05% or 0.25% solution of trypsin with EDTA.

Preliminary experiment. All cell lines under study were seeded onto two 96-well plates: a control plate and a plate subjected to OGD for 4 hours. The percentage of cell death in all three cell lines following OGD treatment was determined by staining fixed cells with DAPI dye, according to the protocol described below. We assessed the need for shorter or longer OGD durations for the C6 and SH-SY5Y cultures and confirmed the subsequent experimental design involving pre-conditioning of the cultures with krypton.

Investigation of krypton protective properties in OGD. The experimental design is shown in Fig. 1. Three cell lines (Ea.Hy926, SH-SY5Y, and C6) were seeded into a single 96-well plate at a density of 10,000 cells per well. Three such plates were used:

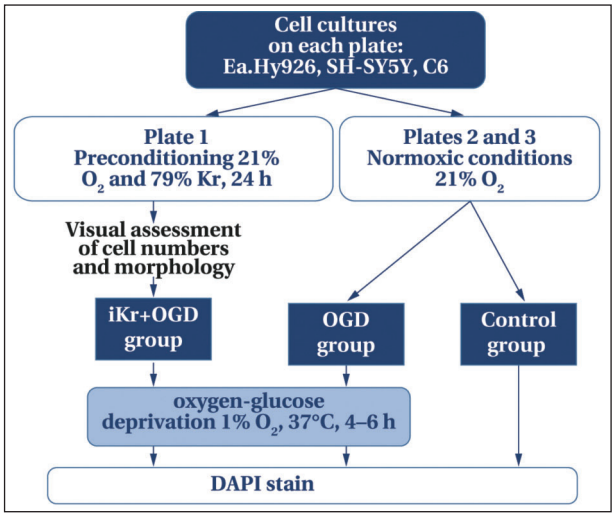

Fig. 1. Study design for NVU cells.

1. iKr+OGD group (cell preconditioning with a krypton-oxygen gas mixture (Kr/O_2 79/21%) (KripOx 79, «InertGas Medical» LLC, Moscow, Russia) for 24 hours, followed by OGD).

2. OGD group (normoxic incubator conditions with oxygen concentration maintained at 21% for 24 hours, followed by OGD).

3. Control group (normoxic incubator conditions with oxygen concentration maintained at 21% throughout the study, without OGD).

Once a monolayer was formed, Plate 1 was transferred to a desiccator filled with the appropriate gas mixture for 24 hours and left in a thermostat to maintain the temperature. Plate 2 was kept in the same incubator under standard normoxic conditions. In this case, the standard CCM for each culture was added to the cells, but only with DMEM and F12 media without sodium bicarbonate. After 24 hours,

the cells in the iKr+OGD and OGD groups were subjected to deprivation. Prior to OGD, a visual assessment was performed to determine whether exposure to the krypton gas mixture had affected cell number and morphology.

Plate 3 was kept in a thermostat under normoxic conditions; the standard culture medium for these cells was added to the cells, but using DMEM and F12 media without sodium bicarbonate.

Modeling of oxygen-glucose deprivation. To induce OGD, the cells were washed three times with DPBS. The cells in DPBS were then transferred to a multi-gas incubator with conditions of 1% O_2, 37°C for 4–6 hours. Subsequently, the cells were supplied with their standard culture medium, consisting of DMEM and F12 without sodium bicarbonate.

After the OGD, the cells were fixed with 4% formaldehyde at room temperature for 15 minutes, then stained with DAPI (300 nM) for 30 minutes. Imaging was performed using a Zeiss fluorescence microscope, followed by analysis in ImageJ.

Statistical analysis of the data was performed using SPSS Statistics software (version 27.0.1; IBM Corp., Armonk, NY, USA) and GraphPad Prism (version 8.0.1; GraphPad Software, Boston, MA, USA). The distribution of variables was tested for normality using the Shapiro–Wilk test. Statistical results were described as *Me* (*Q1*; *Q3*), where *Me* is the median, *Q1* is the 25th percentile, and *Q3* is the 75th percentile. If the distribution differed from the normal in at least one of the groups, nonparametric methods were used: the Mann–Whitney *U* test was applied to analyze differences between two independent samples; when comparing three or more groups, the Mann–Whitney *U* test was used, followed by correction for multiple comparisons using the Holm–Bonferroni method. For the analysis of repeated-measure data with a single factor, the Friedman test was used; when statistically significant differences were detected, a post-hoc analysis was performed using the Wilcoxon test and the Holm–Bonferroni correction for multiple comparisons. Differences between proportions in independent samples were assessed using Pearson's χ^2 test or Fisher's exact test if the expected frequencies were less than 10%. Differences were considered statistically significant at a *p*-value of < 0.05.

Results

Mortality and complications. During the 14-day observation period, 5 animals were withdrawn from the study due to reaching the predefined humane endpoint: 2 animals in the TBI group (18.2%) and 3 animals in the TBI+iKr group (18.8%). No statistically significant differences in the frequency of reaching the humane endpoint were found between the groups ($p=0.677$).

Postoperative inflammatory -necrotizing complications (abscesses) were observed in 1 animal in the TBI group (9.1%) and in 3 animals in the TBI+iKr group (18.8%). No statistically significant differences were found when comparing the incidence of infectious complications between the groups ($p=0.645$, Fisher's exact test).

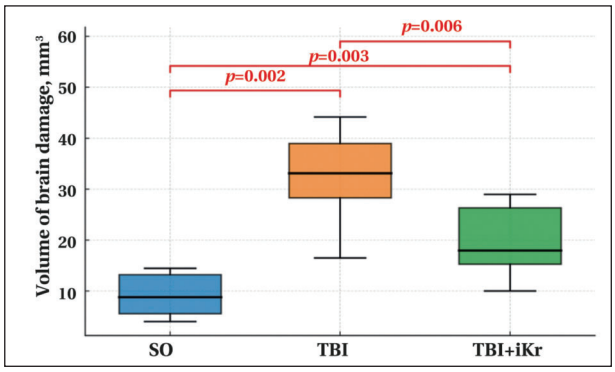

Fig. 2. Extent of brain injury as determined by MRI.
Note. For Figs. 2–4: the rectangles represent the interquartile range (*Q1–Q3*), the center lines represent the median, and the whiskers extend to 1.5 times the interquartile range. Red brackets indicate paired comparisons using the Mann–Whitney test with the Holm–Bonferroni correction; the exact adjusted *p*-values are shown above the brackets.

Animals that reached the humane endpoint or developed infectious complications were excluded from further analysis of long-term outcomes.

MRI scan data. According to MRI findings on day 14, lesions were detected in all groups. A comparison of the three groups revealed statistically significant differences (Kruskal–Wallis test: H = 15.98; $p=0.0003$). The volume of damage differed consistently and statistically significantly in all pairwise comparisons: the median (*Q1*; *Q3*) was 9 (6; 13) mm³ in the SO group, 33 (28; 39) mm³ in the TBI group, and 18 (15; 26) mm³ in the TBI + iKr group (Fig. 2).

Neurological examination. On the third day after simulated TBI, the median total score on the limb placement test (LPT) was 9 (5.5, 10.5) in the SO group, 2.5 (1.25, 4.75) in the TBI group, and 3.5 (2.75, 8.5) in the TBI + iKr group. A comparison of the three groups revealed statistically significant differences (Kruskal–Wallis test: H = 9.62; $p=0.008$). Pairwise comparisons using the Mann–Whitney *U* test and Holm–Bonferroni correction showed a statistically significant decrease in indicators in the TBI group compared to the SO group ($p=0.023$). Differences between the TBI and TBI + iKr groups did not reach statistical significance ($p=0.272$).

On day 7, the values for LPT test were 12 (9.25; 13.3) in the SO group, 2.5 (2.5; 5.25) in the TBI group, and 9 (6; 10.3) in the TBI + iKr group. A general between-group analysis revealed statistically significant differences (H = 10.85; $p=0.004$). Pairwise analysis demonstrated a statistically significant improvement in the TBI + iKr group compared to the

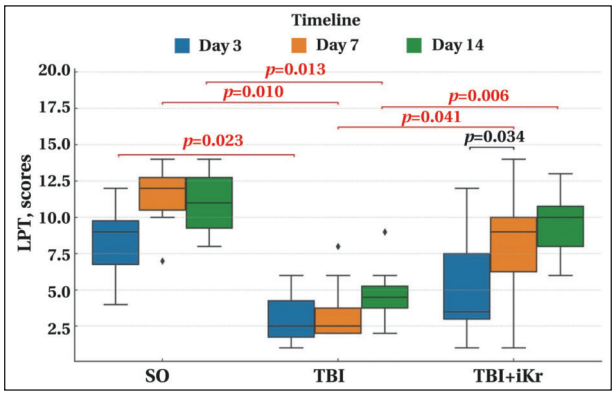

Fig. 3. Results of the limb placement test.
Note. Between-group *p*-values were determined using the Mann–Whitney *U* test, followed by Holm–Bonferroni correction for multiple comparisons (red brackets). Intra-group *p*-values were determined using the Friedman test with a post-hoc analysis by the Wilcoxon test and Holm–Bonferroni correction (black brackets).

TBI group ($p=0.027$), as well as statistically significant differences between the SO and TBI groups ($p=0.012$).

On day 14, the median LPT values were 11 (8.75; 13.3) in the SO group, 4.5 (3.25; 5.75) in the TBI group, and 10 (7.5; 11.3) in the TBI + iKr group. Intergroup differences remained statistically significant (H = 12.73; $p=0.002$). Animals in the TBI + iKr group demonstrated statistically significantly higher scores compared to the TBI group ($p=0.006$), with values approaching those of the SO group (Fig. 3).

An intragroup analysis of changes in LPT scores was performed using the Friedman test. In the SO group, no statistically significant changes in total scores were observed during the observation period ($\chi^2=3.50$; $p=0.1738$). In the TBI group, the changes also did not reach statistical significance ($\chi^2=3.75$; $p=0.1534$). Statistically significant changes in the indicators were found in the TBI + iKr group, ($\chi^2=7.93$; $p=0.019$). A post hoc analysis using the Wilcoxon test and Holm–Bonferroni correction showed a statistically significant improvement between days 3 and 7 ($p\_Holm=0.034$), whereas differences between days 7 and 14 did not reach statistical significance.

Therefore, krypton inhalation was associated with a statistically significant improvement in sensorimotor function beginning on the 7th day after injury, as well as significant positive intra-group trends, which were not observed in the TBI group.

Pro-inflammatory cytokines. Analysis of pro-inflammatory cytokines was performed on the third day following the induction of traumatic brain injury.

Analysis of IL-1β revealed statistically significant differences between the groups (Kruskal–Wallis test: H = 12.28; $p=0.002$). Simulation of traumatic brain injury revealed a statistically significant 2.8-fold increase in the concentration of the pro-inflammatory cytokine IL-1β in the injured cerebral hemisphere — up to 398 (346; 421) pg/g — compared to the intact brains of rats (141 (139; 154) pg/g ($p=0.024$). In the TBI + iKr group, the IL-1β level was statistically significantly reduced by ~51% relative to the TBI group — to 194 (182; 211) pg/g ($p=0.024$), but remained higher than the values in the intact control ($p=0.048$).

Analysis of IL-6 concentrations did not reveal any statistically significant differences between groups (H = 2.96; $p=0.228$). Traumatic brain injury resulted in a statistically insignificant increase in the concentration of the pro-inflammatory cytokine IL-6 to 122 (113; 134) pg/g in the TBI group compared to the intact brain at 101 (92; 121) pg/g ($p=0.234$). In the TBI + iKr group, IL-6 decreased to 102 (96; 112) pg/g, which also did not reach statistical significance compared to the TBI group ($p=0.747$).

Analysis of TNF-α levels revealed statistically significant differences between the groups (H = 12.52; $p=0.002$). TBI led to a statistically significant 2.5-fold increase in TNF-α concentration in the rat brain — up to 205 (188; 243) pg/g versus 83 (77; 91) pg/g in the intact brain ($p=0.024$). In the TBI+iKr group, TNF-α concentration significantly decreased to 112 (112; 123) pg/g compared to the TBI group ($p=0.036$), but also remained higher than control values ($p=0.036$) (Fig. 4).

Histological examination. In the TBI group, histological analysis revealed marked structural abnormalities in both hemispheres. Thickening and partial detachment of the meninges, submeningeal hemorrhages, venous congestion with collapsed vessels, and marked perivascular edema were documented on the contralateral side. A cortical defect extending into the white matter was identified in the ipsilateral hemisphere, complemented by disruption of the meningeal integrity, plasma-filled vascular walls, glial infiltration in the penumbra zone, hemorrhages by diapedesis, and extensive spongiosis extending beyond the penumbra. In the penumbra and intact tissue, numerous dark neurons, shadow cells, and hypochromic neurons were detected.

In the TBI+iKr group, pathological changes were less obvious. The pia mater was thinner and adhered more tightly to the brain surface; submeningeal hemorrhages were detected only sporadically. Perivascular edema and spongiosis were moderately intense, and damaged neurons (dark cells, shadow cells) were encountered less frequently, especially outside the penumbra. Signs of perivascular and periglial edema persisted in the hippocampus, but to a lesser extent than in the TBI group (Fig. 5, *a*).

Inhalation of a krypton-oxygen mixture was associated with reduced edema severity, less extensive spongiosis, and a lower prevalence of degenerative neuronal changes outside the penumbra

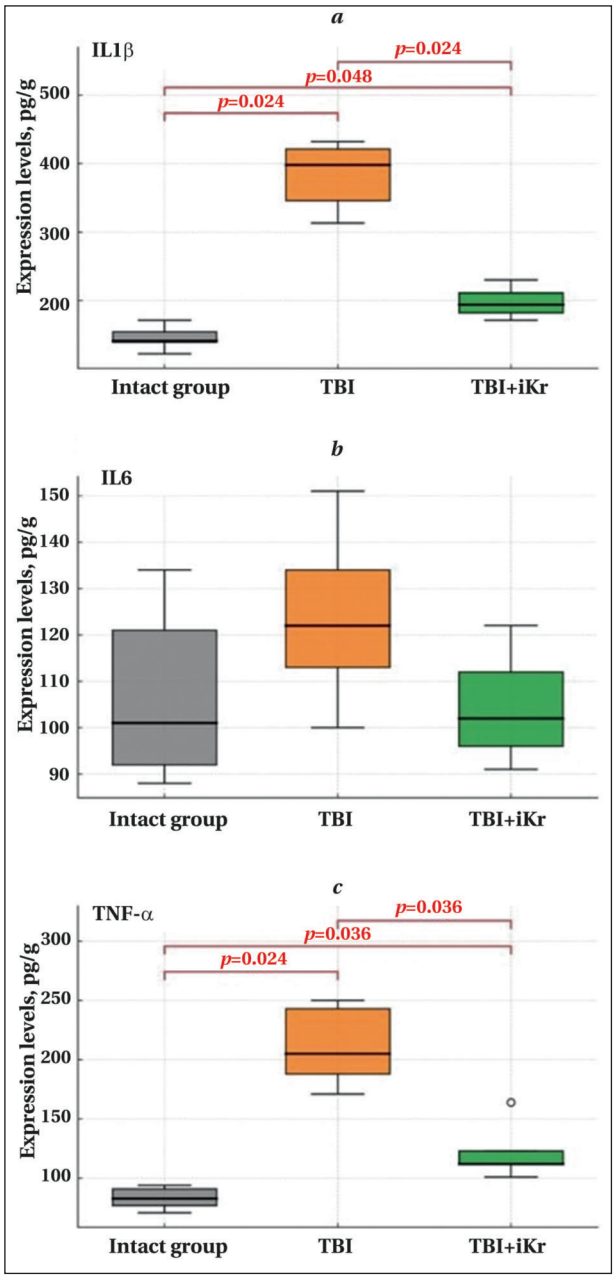

Fig. 4. Levels of pro-inflammatory cytokine expression in the experimental groups.
Note. Red brackets indicate paired comparisons using the Mann–Whitney *U* test, followed by correction for multiple comparisons using the Holm–Bonferroni method; the exact adjusted *p*-values corresponding to the statistical significance thresholds are shown above the brackets.

compared to the TBI group. These data indicate a potential neuroprotective effect of krypton, limiting the spread of structural brain damage following trauma.

Immunohistochemical examination of the brain. To assess the effect of krypton inhalation on cellular responses following traumatic brain injury, a quantitative comparison of GFAP (an astrocyte marker) and caspase-3 (an apoptosis marker) expression was performed in the ipsilateral and contralateral hemispheres of the brain.

Immunohistochemical analysis revealed a typical increase in GFAP expression in the ipsilateral hemisphere compared to the contralateral hemisphere, reflecting the development of gliosis in the injury zone in the TBI group. In the TBI + iKr group, GFAP expression activity in the ipsilateral zone was higher than in animals in the TBI group, with no differences on the contralateral side. Statistical analysis showed a trend toward increased GFAP levels in the TBI + iKr group ($p = 0.086$) with no differences for Caspase-3 or contralateral values ($p = 0.629$).

To clarify the nature of the changes, we calculated the differences between the sides (△GFAP and △Caspase-3), reflecting the degree of asymmetry in expression. The analysis showed that △GFAP in the TBI + iKr group was higher than in the TBI group ($p = 0.086$), which confirmed the effect of krypton on enhancement of gliosis. △Caspase-3 values did not differ between the groups ($p > 0.999$), indicating that krypton had no effect on the severity of apoptosis by the 14th day of observation. Thus, krypton inhalation following TBI was accompanied by increased gliosis, without exerting a significant effect on neuronal apoptotic activity (Fig. 5, *b*).

Results of the *in vitro* study. No statistically significant differences were found between the groups in the study of the protective effects of preconditioning with a krypton-oxygen breathing mixture on the survival of cell cultures comprising the NVU. The percentage of surviving neuronal cells (SH-SY5Y) after OGD relative to normoxia in the control group was 17.2 (14.6; 18.53)%, and in the krypton group, 16.2 (9.02; 20.1)% ($p = 0.813$) (Fig. 6, *a*). The survival of cells of endothelial and glial origin also did not significantly improve under the influence of krypton, and the percentage of surviving cells was 77.6 (72.6; 89.9)% versus 69.8 (63.7; 84.8)% ($p = 0.199$) in the Ea.Hy culture (Fig. 6, *b*) and 66.5 (57.9; 77.1)% versus 60.4 (57.6; 64.2)% ($p = 0.160$) in the C6 culture (Fig. 6, *c*).

Discussion

The main finding of the study was the significant neuroprotective effect of krypton in an *in vivo* model of traumatic brain injury, as evidenced by both morphological data (MRI and histological examination) and functional tests (LPT). Furthermore, PCR data confirmed the anti-inflammatory nature of krypton's neuroprotective effect.

However, in vitro studies did not reveal any protective effects of krypton on any of the components of the NVU, which underscores the effectiveness of this inert gas only within the intact organism, but not in isolated cells.

The IHC study confirmed previous findings that the number of GFAP-positive cells in the injury zone increases in the delayed phase following in-

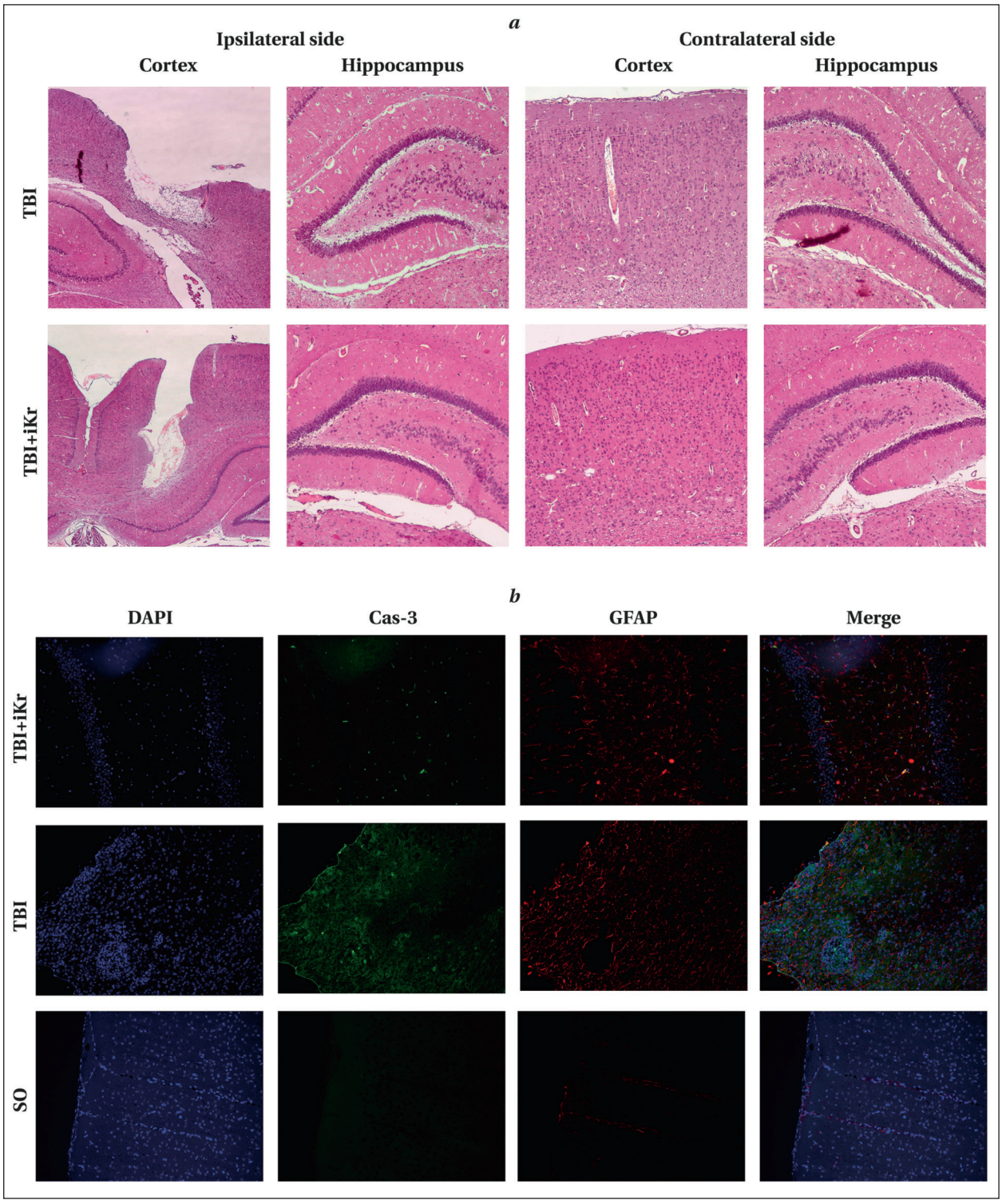

Fig. 5. Histological (*a*) and immunohistochemical (*b*) analysis of rat brain tissue following traumatic brain injury.
Note. *a* — Hematoxylin-eosin staining; *b* — Fluorescent immunohistochemical staining of the rat cerebral cortex. Blue — total number of DAPI-positive nuclei; Green — immune-labeled activated caspase-3 (Cas-3); Red color — immune-labeled astrocyte intermediate filaments (astrocytic glia, marker of reactive gliosis); Merge — overlay of all three channels. 20× magnification.

jury [40]. A higher number of GFAP-positive cells was also observed in the TBI + iKr group.

Although there is very little data on the neuroprotective effects of krypton [38, 40], given our previous studies [31, 41] using models of photochemically induced stroke, it can be assumed that the neuroprotective effects of krypton also apply to traumatic brain injury. Of course, these results require further in-depth analysis to determine optimal concentrations and treatment regimens, as well as to clarify the molecular mechanisms underlying the observed effects. Nevertheless, the con-

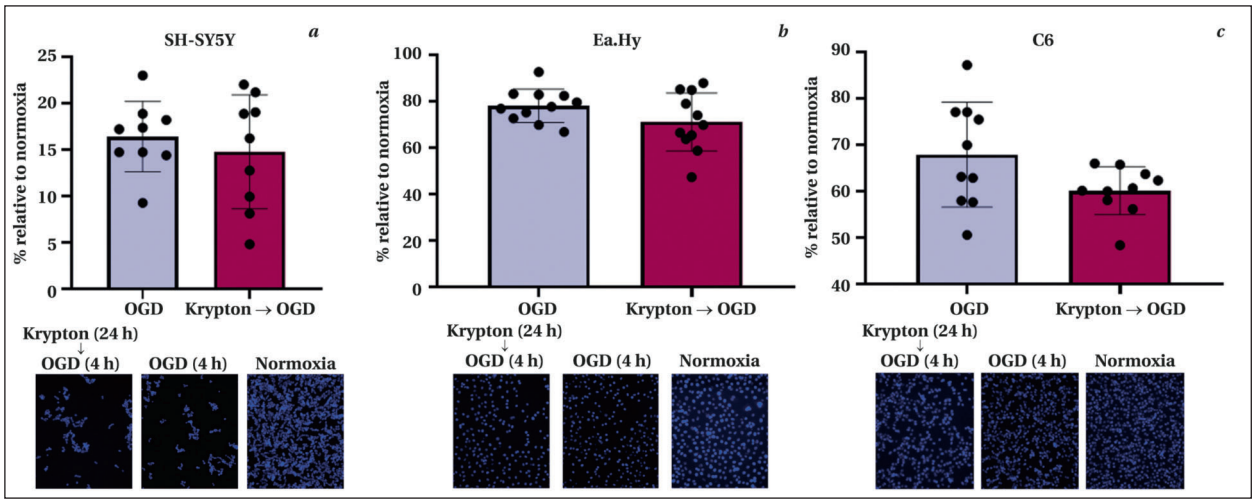

Fig. 6. Cells of neural origin (SH-SY5Y, *a*), vascular endothelial cells (Ea.Hy, *b*), and glial cells (C6, *c*).

sistent neuroprotective effect of krypton in models of brain injury of various etiologies may inspire researchers to expand the scope of studies on krypton-oxygen therapy.

It is worth noting that krypton and xenon not only share similar physicochemical properties but also exhibit similar biological effects, as demonstrated in *in vivo* studies [38, 42]. However, the results of *in vitro* studies [40, 43] show that, on isolated cells, krypton is capable not only of failing to exert a positive effect in cases of brain injury, but also of reducing the nerve cells resistance to hypoxia. Thus, in the absence of OGD, krypton reduced the regenerative capacity of intact cells ($p < 0.01$), which was not observed in studies with xenon or argon [40]. These data do not diminish krypton's neuroprotective potential but merely justify a differential approach to studying the molecular mechanisms of action of inert gases.

Any pathological process develops over time and progresses through successive stages, a fact that must be taken into account when planning therapeutic interventions. The efficacy of the same agent can vary significantly depending on the phase of injury: an intervention that has a pronounced positive effect within the therapeutic window (e.g., thrombolysis in ischemic stroke) may, under other conditions, become neutral or even detrimental. This stage-dependent behavior likely explains the variability in the effects of inert gases when modeling the same pathology. Therefore, in the therapeutic application of inert gases, one should take into account both the characteristics of the agent itself and the nature and phases of the pathological process [44].

Conclusion

Krypton suppresses secondary damage in a rat model of traumatic brain injury, reduces neurological deficits during the first 14 days of observation, and reduces the volume of damage as determined by MRI. Beneficial effects of krypton gas are attributed to the suppression of the inflammatory process as demonstrated by a significant reduction in the mRNA levels of IL-1β and TNF-α pro-inflammatory cytokines. However, no neuroprotective effect of krypton was observed *in vitro*. This duality and ambiguity of the results necessitate further investigation into the role of the whole organism in the manifestation of krypton's neuroprotective effects.

References

1. *Guan B., Anderson D., Chen L., Feng S., Zhou H.* Global, regional and national burden of traumatic brain injury and spinal cord injury, 1990-2019: a systematic analysis for the Global Burden of Disease Study 2019. *BMJ Open*. 2023; 13 (10): e075049. DOI: 10.1136/bmjopen-2023-075049. PMID: 37802626.
2. *Silvestro S., Raffaele I., Quartarone A., Mazzon E.* Innovative insights into traumatic brain injuries: biomarkers and new pharmacological targets. *Int J Mol Sci*. 2024; 25 (4): 2372. DOI: 10.3390/ijms25042372. PMID: 38397046.
3. Ассоциация нейрохирургов России. Очаговая травма головного мозга. Клинические рекомендации. М.; 2022: 82. Association of Neurosurgeons of Russia. Focal Brain Injury. Clinical Guidelines. Moscow; 2022: 82.
4. *Lewis A.* Neurocritical care. *Continuum: Lifelong Learning in Neurology*. 2024; 30 (3): e7–e31. DOI: 10.1212/CON.0000000000001460.
5. *Lavinio A., Coles J., Robba C., Aries M., Bouzat P., Chean D., Frisvold S., et al.* Targeted temperature control following traumatic brain injury: ESICM/NACCS best practice consensus recommendations. *Crit Care*. 2024; 28 (1): 170. DOI: 10.1186/s13054-024-04951-x. PMID: 38769582.
6. *Bernard F.* Neurotrauma and intracranial pressure management. *Crit Care Clin*. 2023; 39: 103–21. DOI: 10.1016/j.ccc.2022.08.002. PMID: 36333026.
7. *Dietvorst S., Depreitere B., Meyfroidt G.* Beyond intracranial pressure: monitoring cerebral perfusion and autoregulation in severe traumatic brain injury. *Curr Opin Crit Care*. 2023; 29: 85–88. DOI: 10.1097/MCC.0000000000001026. PMID: 36762674.
8. *Kundu S., Singh S.* What happens in TBI? A wide talk on animal models and future perspective. *Curr Neuropharmacol*. 2023; 21: 1139. DOI: 10.2174/1570159X20666220706094248. PMID: 35794772.
9. *Haupt M., Gerner S., Bähr M., Doeppner T. R.* Neuroprotective strategies for ischemic stroke — future perspectives. *Int J Mol Sci*. 2023; 24 (5): 4334. DOI: 10.3390/ijms24054334. PMID: 36901765.
10. *Buccilli B., Alan A., Baha A., Shahzad A., Almealawy Y. F., Chisvo N.S., Ennabe M. et al.* Neuroprotection strategies in traumatic brain injury: Studying the effectiveness of different clinical approaches. *Surg Neurol Int*. 2024; 15: 29. DOI: 10.25259/SNI_773_2023. PMID: 38344087.
11. *Carbonara M., Fossi F., Zoerle T., Ortolano F., Moro F., Pischiutta F., Zanier E. R., et al.* Neuroprotection in traumatic brain injury: sesenchymal Stromal cells can potentially overcome some limitations of previous clinical trials. *Front Neurol*. 2018; 9: 885. DOI: 10.3389/fneur.2018.00885. PMID: 30405517.
12. *Maas A.* Neuroprotective agents in traumatic brain injury. *Expert Opin Investig Drugs*. 2001; 10: 753–767. DOI: 10.1517/13543784.10.4.753. PMID: 11281824.
13. *Chen J., Jin J., Li K., Shi L., Wen X., Fang F.* Progresses and prospects of neuroprotective agents-loaded nanoparticles and biomimetic material in ischemic stroke. *Front Cell Neurosci*. 2022; 16: 868323. DOI: 10.3389/fncel.2022.868323. PMID: 35480961.
14. *Kato R., Zhang L., Kinatukara N., Huang R., Asthana A., Weber C., Xia M., et al.* Investigating blood-brain barrier penetration and neurotoxicity of natural products for central nervous system drug development. *Sci Rep*. 2025; 15 (1): 7431. DOI: 10.1038/s41598-025-90888-2. PMID: 40032960.
15. *Tong M., Li X., Cheng J., Jiang Z.-L.* Developments in the study of inert gas biological effects and the underlying molecular mechanisms. *Int J Mol Sci*. 2025; 26 (15): 7551. DOI: 10.3390/ijms26157551. PMID: 40806678.
16. *Reyes-Figueroa A., Karttunen M., Ruiz-Suárez J.* Cholesterol sequestration by xenon nano bubbles leads to lipid raft destabilization. *Soft Matter*. 2020; 16: 9655–61. DOI: 10.1039/d0sm01256d. PMID: 33078812.
17. *Spaggiari S., Kepp O., Rello-Varona S., Chaba K., Adjemian S., Pype J., Galluzzi L., et al.* Anti-apoptotic activity of argon and xenon. *Cell Cycle*. 2013; 12 (16): 2636–42. DOI: 10.4161/cc.25650. PMID: 23907115.
18. *Melnikov I., Orekhov P., Rulev M., Kovalev K., Astashkin R., Bratanov D., Ryzhikay Yu., et al.* High-pressure crystallography shows noble gas intervention into protein-lipid interaction and suggests a model for anaesthetic action. *Commun Biol*. 2022; 5 (1): 360. DOI: 10.1038/s42003-022-03233-y. PMID: 35422073.
19. *Боева Е. А., Сутормин М. В., Антонова В. В., Любомудров М. А., Черпаков Р. А., Лобанов А. В., Кузовлев А.Н с соавт.* Изучение нейропротективного действия аргон-кислородной смеси при ингаляции через 24 часа после ишемического инсульта. *Патологическая физиология и экспериментальная терапия*. 2025; 69 (2): 38–45. *Boeva E. A., Sutormin M. V., Antonova V. V., Lyubomudrov M. A., Cherpakov R. A., Lobanov A. V., Kuzovlev A. N., et al.* The study of argon-oxygen mixture neuroprotective effect when inhaled 24 hours after ischemic stroke. *Pathological Physiology and Experimental Therapy = Patologicheskaya Fiziologiya i Exsperimentalnaya Terapiya*. 2025; 69 (2): 38–45. DOI: 10.48612/pfiet/0031-2991.2025.02.38-45.

20. *Preckel B., Weber N. C., Sanders R. D., Maze M., Schlack W.* Molecular mechanisms transducing the anesthetic, analgesic, and organ-protective actions of xenon. *Anesthesiology*. 2006; 105 (1): 187–197. DOI: 10.1097/00000542-200607000-00029. PMID: 16810011.
21. *Sanders R., Ma D., Maze M.* Xenon: elemental anaesthesia in clinical practice. *Br Med Bull*. 2005; 71: 115–35. DOI: 10.1093/bmb/ldh034. PMID: 15728132.
22. *Сафиуллин Д. Р., Шабанов А. К., Гринь А. А., Черпаков Р. А., Евсеев А. К., Евдокимов А. И., Петриков С. С. с соавт.* Безопасность применения продленной седации севофлураном у пациентов с тяжелой черепно-мозговой травмой. *Журнал им. Н.В. Склифосовского Неотложная медицинская помощь*. 2024; 13 (2): 312–321. *Safiullin D. R., Shabanov A. K., Grin A. A., Cherkapov R. A., Evseev A. K., Evdokimov A. I., Petrikov S. S., et al.* Safety of extended sedation with sevoflurane in patients with severe traumatic brain injury. *Russian Sklifosovsky Journal «Emergency Medical Care» = Zhurnal im. N.V. Sklifosovskogo «Neotlozhnaya Meditsinskaya Pomoshch»*. 2024; 13 (2): 312–321. (in Russ.). DOI: 10.23934/2223-9022-2024-13-2-312-321.
23. *Jolliet P., Ouanes-Besbes L., Abroug F., Khelil J. B., Besbes M., Garnero A., Arnal J.-M., et al.* A multicenter randomized trial assessing the efficacy of helium/oxygen in severe exacerbations of chronic obstructive pulmonary disease. *Am J Respir Crit Care Med*. 2017; 195 (7): 871–80. DOI: 10.1164/rccm.201601-0083OC. PMID: 27736154.
24. *Nascimento M., Santos É., Prado C. D.* Helium-oxygen mixture: clinical applicability in an intensive care unit. *Einstein (Sao Paulo)*. 2018; 16: eAO4199. DOI: 10.31744/einstein_journal/2018AO4199. PMID: 30427479.
25. *Merigo G., Magliocca A., Florio G., Madotto F.* Inhaled argon as a neuroprotective agent after an ischemic event — a fully translational story from animal studies to a human trial. *Vascul Pharmacol*. 2024; 155: 107333. DOI: 10.1016/j.vph.2024.107333.
26. *Merigo G., Florio G., Madotto F., Magliocca A., Silvestri I., Fumagalli F., Cerrato M., et al.* Treatment with inhaled argon: a systematic review of pre-clinical and clinical studies with meta-analysis on neuroprotective effect. *eBioMedicine*. 2024; 103: 105143. DOI: 10.1016/j.ebiom.2024.105143. PMID: 38691938.
27. *González T. S., Delbrel A., Giacomino L., Meunier D., Sein J., Renaud L., Brige P., et al.* Long lasting argon neuroprotection in a non-human primate model of transient endovascular ischemic stroke. *J Cereb Blood Flow Metab*. 2025; 45 (4): 643–54. DOI: 10.1177/0271678X241297798. PMID: 39628320.
28. *Bao L., Liu Y., Jia Q., Chu S., Jiang H., He S.* Argon neuroprotection in ischemic stroke and its underlying mechanism. *Brain Res Bull*. 2024; 212: 110964. DOI: 10.1016/j.brainresbull.2024.110964. PMID: 38670471.
29. *Antonova V. V., Silachev D. N., Ryzhkov I. A., Lapin K. N., Kalabushev S. N., Ostrova I. V., Varnakova L. A., et al.* Three-hour argon inhalation has no neuroprotective effect after open traumatic brain injury in rats. *Brain Sci*. 2022; 12 (7): 920. DOI: 10.3390/brainsci12070920. PMID: 35884727.
30. *Creed J., Cantillana-Riquelme V., Yan B. H., Ma S., Chu D., Wang H., Turner D. A., et al.* Argon inhalation for 24 h after closed-head injury does not improve recovery, neuroinflammation, or neurologic outcome in mice. *Neurocrit Care*. 2021; 34 (3): 833–43. DOI: 10.1007/s12028-020-01104-0. PMID: 32959200.
31. *Antonova V. V., Silachev D. N., Plotnikov E. Y., Pevzner I. B., Yakupova E. I., Pisarev M. V., Noeva E. A., et al.* Neuroprotective effects of krypton inhalation on photothrombotic ischemic stroke. *Biomedicines*. 2024; 12 (3): 635. DOI: 10.3390/biomedicines12030635. PMID: 38540249.
32. *Шумов И. В., Антонова В. В., Боева Е. А., Долгих В. Т., Гребенчиков О. А.* Нейропротекторные свойства криптона при фотоиндуцированном инфаркте головного мозга у крыс. *Вестник СурГУ. Медицина*. 2023; 16 (3): 89–96. *Shumov I. V., Antonova V. V., Boeva E. A., Dolgikh V. T., Grebencchikov O. A.* Neuroprotective properties of krypton in photoinduced cerebral infarction in rats. *Bulletin of Surgut State University. Medicine = Vestnik SurGU. Meditsina*. 2023; 16 (3): 89–96. (in Russ.). DOI: 10/35266/2304-9448-2023-3-89-96.
33. *Feeney D. M., Boyeson M. G., Linn R. T., Murray H. M., Dail W. G.* Responses to cortical injury: I. Methodology and local effects of contusions in the rat. *Brain Res*. 1981; 211 (1): 67–77. DOI: 10.1016/0006-8993 (81)90067-6. PMID: 7225844.
34. *De Ryck M., Van Reempts J., Borgers M., Wauquier A., Janssen P. A.* Photochemical stroke model: flunarizine prevents sensorimotor deficits after neocortical infarcts in rats. *Stroke*. 1989; 20 (10): 1383–90. DOI: 10.1161/01.str.20.10.1383. PMID: 2799870.
35. *Jolkkonen J., Puurunen K., Rantakömi S., Härkönen A., Haapalinna A., Sivenius J.* Behavioral effects of the α2-adrenoceptor antagonist, atipamezole, after focal cerebral ischemia in rats. *Eur J Pharmacol*. 2000; 400 (2–3): 211–219.

DOI: 10.1016/s0014-2999 (00)00409-x.
PMID: 10988336.

36. *Antonova V. V., Silachev D. N., Plotnikov E. Y., Pevzner I. B., Ivanov M. E., Boeva E. A., Kalabushev S. N., et al.* Positive effects of argon inhalation after traumatic brain injury in rats. *Int J Mol Sci*. 2024; 25 (23): 12673.
DOI: 10.3390/ijms252312673. PMID: 39684384.
37. *Силачев Д. Н., Учеваткин А. А., Пирогов Ю. А.* Сравнительная оценка двух методов исследования экспериментальной фокальной ишемии: магнитно-резонансной томографии и трифенилтетразолиевой детекции повреждений головного мозга. *Бюллетень экспериментальной биологии и медицины*. 2009; 147: 269–272. *Silachev D. N., Uchevatkin A. A., Pirogov Yu. A.* Comparative evaluation of two methods for studying experimental focal ischemia: magnetic resonance imaging and triphenyltetrazolium detection of brain damage. *Bulletin of Experimental Biology and Medicine = Biulletten Eksperimentalnoy Biologii i Meditsiny*. 2009; 147: 269–272. (in Russ.).
38. *Flin R., Winter J., Sarac C., Raduma M.* Human factors in patient safety: review of topics and tools. Report for Methods and Measures Working Group of WHO Patient Safety. Geneva: World Health Organization; 2009.
39. *Солдатов П. Э., Шулагин Ю. А., Тюрин-Кузьмин А. Ю., Дьяченко А. И.* Устойчивость к гипоксической гипоксии после предварительного воздействия нормоксических дыхательных смесей, содержащих аргон или криптон. *Авиакосмическая и экологическая медицина*. 2021; 55 (3): 74–80. 39. *Soldatov P. E., Shulagin Yu.A., Tyurin-Kuzmin A.Yu., Dyachenko A. I.* Endurance of hypoxic hypoxia after preliminary breathing of normoxic mixtures containing argon or krypton. *Aerospace and Environmental Medicine = Aviakosmicheskaya i Ekologicheskaya Meditsina*. 2021; 55 (3): 74–80. (in Russ.).
DOI: 10.21687/0233-528X-2021-55-3-74-80.
40. *Jawad N., Rizvi M., Gu J., Adeyi O., Tao G., Maze M., Ma D.* Neuroprotection (and lack of neuroprotection) afforded by a series of noble gases in an in vitro model of neuronal injury. *Neurosci Lett*. 2009; 460 (3): 232–236.
DOI: 10.1016/j.neulet.2009.05.069.
PMID: 19500647.
41. *Антонова В. В., Шумов И. В., Долгих В. Т., Гребенчикова А. А., Габитов М. В., Якупова Э. И., Гребенчиков О. А.* Влияние дыхания криптон-кислородной смесью на сигнальные каскады в мозге крыс при моделировании фотоиндуцированного ишемического инсульта. *Бюллетень экспериментальной биологии и медицины*. 2024; 178 (9): 321–327. *Antonova V. V., Shumov I. V., Dolgikh V. T., Grebencchikova A. A., Gabitov M. V., Yakupova E. I., Grebencchikov O. A.* Influence of breathing krypton-oxygen mixture on signaling cascades in the rat brain in the simulation of photoinduced ischemic stroke. *Bulletin of Experimental Biology and Medicine = Biulletten Eksperimentalnoy Biologii i Meditsiny*. 2024; 178 (9): 321–327. (in Russ.).
DOI: 10.47056/0365-9615-2024-178-9-321-327.
42. *Schiltz M., Shepard W., Fourme R., Prange T., de la Fortelle E., Bricogne G.* High-pressure krypton gas and statistical heavy-atom refinement: a successful combination of tools for macromolecular structure determination. *Acta Crystallogr D Biol Crystallogr*. 1997; 53 (Pt 1): 78–92.
DOI: 10.1107/S0907444996009705.
PMID: 15299973.
43. *Koziakova M., Harris K., Edge C. J., Franks N. P., White I. L., Dickinson R.* Noble gas neuroprotection: xenon and argon protect against hypoxic–ischaemic injury in rat hippocampus in vitro via distinct mechanisms. *Br J Anaesth*. 2019; 123 (5): 601–609.
DOI: 10.1016/j.bja.2019.07.010. PMID: 31470983.
44. *Боева Е. А., Гребенчиков О. А.* Органопротективные свойств аргона (обзор). *Общая реаниматология*. 2022; 18 (5): 44–59. *Boeva E. A., Grebencchikov O. A.* Organoprotective properties of argon (Review). *General Reanimatology = Obshchaya Reanimatologiya*. 2022; 18 (5): 44–59. (in Russ.&Eng.).
DOI: 10.15360/1813-9779-2022-5-44-59.

Received 04.12.2025
Accepted 08.04.2026
Online First 09.04.2026